Separation Science and Technology
Publication details, including instructions for authors and subscription information:
http://www.informaworld.com/smpp/title~content=t713708471

Synthesis of High Surface Area $MgAl_2O_4$ Nanopowder as Adsorbent for Leather Dye Removal

Edson Luiz Foletto[a]; Sérgio Luiz Jahn[a]; Regina de Fátima Peralta Muniz Moreira[b]
[a] Department of Chemical Engineering, Federal University of Santa Maria, Santa Maria, RS, Brazil [b] Department of Chemical and Food Engineering, Federal University of Santa Catarina, Florianópolis, SC, Brazil

To cite this Article Foletto, Edson Luiz , Jahn, Sérgio Luiz and Muniz Moreira, Regina de Fátima Peralta(2009) 'Synthesis of High Surface Area $MgAl_2O_4$ Nanopowder as Adsorbent for Leather Dye Removal', Separation Science and Technology, 44: 9, 2132 — 2145
To link to this Article: DOI: 10.1080/01496390902775620
URL: http://dx.doi.org/10.1080/01496390902775620

Separation Science and Technology, 44: 2132–2145, 2009

ISSN: 0149-6395 print/1520-5754 online
DOI: 10.1080/01496390902775620

Taylor & Francis
Taylor & Francis Group

Synthesis of High Surface Area $MgAl_2O_4$ Nanopowder as Adsorbent for Leather Dye Removal

Edson Luiz Foletto,[1] Sérgio Luiz Jahn,[1] and Regina de Fátima Peralta Muniz Moreira[2]
[1]Department of Chemical Engineering, Federal University of Santa Maria, Santa Maria, RS, Brazil
[2]Department of Chemical and Food Engineering, Federal University of Santa Catarina, Florianópolis, SC, Brazil

Abstract: $MgAl_2O_4$ nanopowder has been prepared by alkoxides hydrolysis with further calcination at temperature of 700°C. The adsorption of a leather dye, Direct Black 38, onto this material was investigated. The sample was characterized by X-ray-diffraction (XRD), N_2 adsorption–desorption isotherm and Fourier transform infrared spectroscopy. The results showed that sample present a pure phase, and the average nanocrystal size of 8 nm, the BET surface area is about 206.5 $m^2 \cdot g^{-1}$ and total pore volume is about 1.44 $cm^3 \cdot g^{-1}$. Adsorption kinetics data were modeled by film and pore diffusion model. The experimental isotherm was described by the Langmuir model. $MgAl_2O_4$ nanopowder presented a great removal efficiency of leather dye by adsorption process, with a maximum adsorption capacity of 833 mg of dye per gram of adsorbent.

Keywords: Adsorption, dye, isotherm, kinetics, $MgAl_2O_4$, synthesis

INTRODUCTION

The discharge of dyes in the aquatic environmental generate severe pollution problems by inhibiting photosynthetic activity (1).

Received 23 June 2008; accepted 9 January 2009.
Address correspondence to Edson Luiz Foletto, Department of Chemical Engineering, Federal University of Santa Maria, Santa Maria, RS 97105-900, Brazil. E-mail: foletto@smail.ufsm.br

Conventionally, dye wastewater discharged by the textile industry are treated with various chemical and physical methods, such as chemical coagulation, biological treatment, adsorption, ultrafiltration, and photocatalytic treatment (2–6). Among several chemical and physical methods, the adsorption has been found to be superior compared to other techniques for wastewater treatment in terms of its capability for efficiently adsorbing a broad range of adsorbates and its simplicity of design (7). Synthetic organic dye adsorption by solid materials has been extensively studied by many researchers (8–14). However, the search for novel materials in adsorption process with high performance has been a matter of interest in the last years.

Spinel is a ternary oxide with a chemical formula of AB_2O_4, where A is a divalent metallic cation in a tetrahedral site and B is a trivalent metallic cation in an octahedral site of the cubic structure. Magnesium aluminate spinel ($MgAl_2O_4$) has a specific combination of desirable properties such as: high melting point (2135°C), high resistance to chemical attack, good mechanical strength from room temperature to high temperatures, low dielectric constant, excellent optical properties, low thermal expansion, and good catalytic properties (14–17). Conventionally, the spinel ($MgAl_2O_4$) is prepared through a reaction in the solid state using MgO and Al_2O_3 (18,19). In this process, the mixture is calcined at high temperatures such as 1400–1600°C. An effort to synthesize $MgAl_2O_4$ at lower temperatures has been reached by using chemical synthesis processes, especially chemical co-precipitation (20) and sol–gel processes (21,22), where the spinel phase is formed at temperatures around 700°C. Due to its wide and varied applications, the synthesis and properties of $MgAl_2O_4$ have been the focus of recent research.

In the present work, $MgAl_2O_4$ nanopowder was synthesized by alkoxides hydrolysis with further calcination at temperature of 700°C. The performance of the solid was investigated in the removal of black azo dye by adsorption process.

EXPERIMENTAL

Synthesis of the Spinel

The following reactants were utilized: aluminium isopropoxide $[(CH_3)_2CHO]_3Al$ and magnesium ethoxide $(C_2H_5O)_2Mg$, both from Aldrich (purity >98%). For the synthesis, two solutions 0.2 M of metallic alkoxides were prepared using alcohols as the solvent. The first solution was prepared by dissolving 62.8 g of aluminium isopropoxide (0.308 mol) in 1540 mL of isopropanol and the second one was prepared by dissolving

12.56 g of magnesium ethoxide (0.110 mol) in 550 mL of methanol. Both solutions were mixed in a 5 L beaker, then heated to the methanol boiling point and under vigorous stirring 330 mL of water was added. After adding water, the system was kept under heating and stirring for 3 h to complete the hydrolysis reaction. The formed material was separated from the alcohols by filtration and further dried in an oven at 120°C for 24 h, resulting in a fine powder. This fine powder (a mixture of Mg and Al hydroxides) was put in a 100 mesh sieve and calcined in an oxidizing atmosphere (air) at temperature of 700°C, for 4 h, to form the $MgAl_2O_4$ spinel phase.

Characterization Methods

Nanopowder was characterized by X-ray diffractometry (XRD) (equipment Shimadzu model XD-7, with Cu Kα radiation). The average size of the $MgAl_2O_4$ spinel crystallite was determined through the Scherrer equation (using silicon as standard): $D = K \cdot \lambda / (h_{1/2} \cdot \cos\theta)$, where D is the average crystallite size, K the Scherrer constant (0.9×57.3), λ the wavelength of incident X-rays (0.15405 nm), $h_{1/2}$ the peak width at half height and θ corresponds to the peak position (in this work, $2\theta = 36.89$).

Fourier transform infrared spectroscopy (FTIR) spectra were recorded with a Perkin Elmer 883 infrared spectrophotometer.

N_2 adsorption–desorption isotherm measurements were carried out at 77 K using a Autosorb (Quantachrome) apparatus. Specific surface area determination were evaluated in the equilibrium points P/P_0 range from 0.1 to 0.99 by BET method.

Adsorption Study

Direct Black 38, an azo dye extensively used in the leather industry, was used as a model compound. The chemical structure of the dye is given in Fig. 1.

For adsorption tests, 0.2 g of the adsorbent was added to 200 mL of the aqueous solution of dye at different initial concentrations and at pH = 2.5. The pH = 2.5 was adjusted by using dilute H_2SO_4. The resulting solution was then stirred continuously at constant temperature (25 ± 2°C) in the dark to achieve the adsorption equilibrium of dye on the solid. During the runs 5 mL samples of solution were withdrawn at regular intervals and were centrifuged and filtered through a 0.22 µ PVDF membrane (Millipore) to completely remove solid particles. The amount of adsorbed dye on the solid surface was determined by mass balance. UV-vis absorption spectrum of Direct Black 38 aqueous

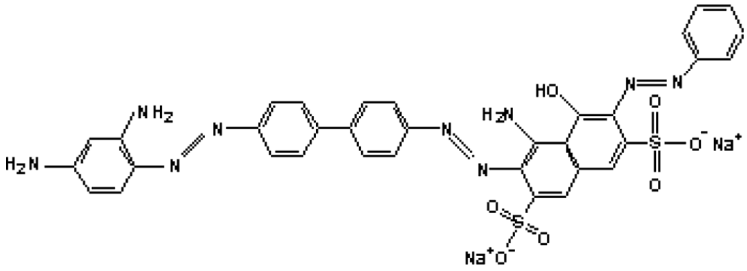

Figure 1. Chemical structure of azo dye.

solution at pH 2.5 is shown in previous work (23). All samples were analyzed using a Shimadzu 1650C UV spectrophotometer at $\lambda_{max.} = 590\,nm$.

RESULTS AND DISCUSSIONS

Spinel Characterization

The XRD pattern for $MgAl_2O_4$ is shown in Fig. 2. All the diffraction peaks can be perfectly indexed to cubic spinel-structured $MgAl_2O_4$ (JCPDS Card No. 77-1203). The peaks and intensities of the produced

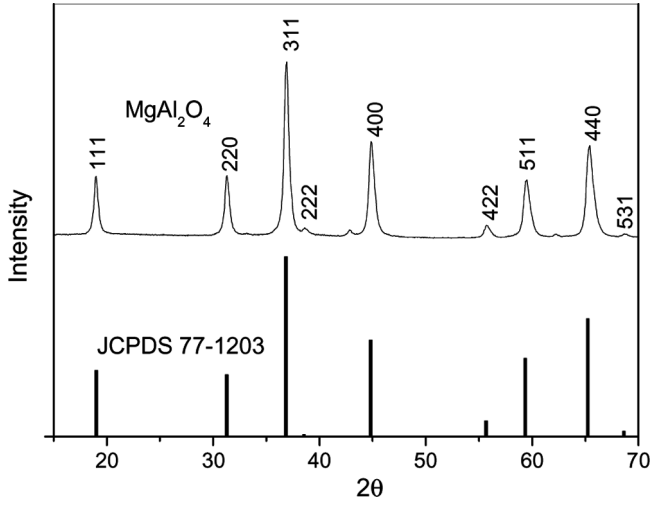

Figure 2. Powder XRD pattern of $MgAl_2O_4$ and reference $MgAl_2O_4$ (JCPDS Card No. 77-1203).

powder and that of standard were the same. This indicates that there is a complete formation of spinel phase in the calcined sample at 700°C. The lattice constant obtained by refinement of XRD data for the synthesized $MgAl_2O_4$ was $a = 8.08\,Å$ and is in good agreement with the literature value (JCPDS Card No. 77-1203). The average crystalline size is about 8 nm, determined by Scherrer equation.

Figure 3 shows the IR spectra of sample calcined at 700°C. Broad OH^- band centered around $3400\,cm^{-1}$, and the $1630\,cm^{-1}$ correspond to H_2O vibration band. Bands around 690 and $530\,cm^{-1}$ are found, and these bands correspond to the existence of AlO_6 groups building up the magnesium spinel, and indict the formation of $MgAl_2O_4$ spinel for the synthesized sample (24,25).

Representation of nitrogen adsorption–desorption isotherm for sample of magnesium aluminate calcined at 750°C is shown in Fig. 4. The isotherm can be classified as type II. The absence of hysteresis is typical for solids that not present mesoporosity. The BET area surface of $206.5\,m^2 \cdot g^{-1}$ was calculated, and the total pore volume was $1.44\,cm^3 \cdot g^{-1}$. A modified sol-gel route, by combining the gelation and the coprecipitation process, was developed for the synthesis of high surface area $MgAl_2O_4$ spinel (25). The surface area reaches levels between 151 and $205\,m^2 \cdot g^{-1}$. Compared to the conventional method that mixed MgO and Al_2O_3, then sintered them at 1400–1600°C to obtained $MgAl_2O_4$ (18,19), the synthetic route employed in this work has excellent

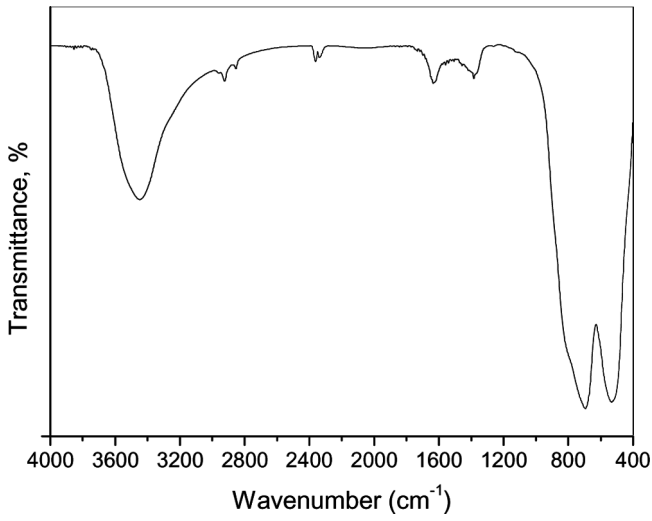

Figure 3. IR spectra of $MgAl_2O_4$ spinel calcined at 700°C.

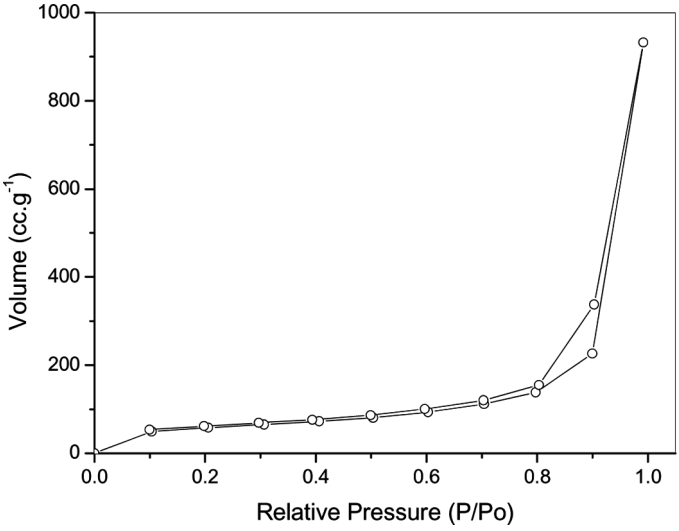

Figure 4. Nitrogen adsorption–desorption isotherm for $MgAl_2O_4$ spinel calcined at 700°C.

advantages to obtain high crystalline powders with great specific surface area, nanometric particle size and high purity at lower temperatures of synthesis. The values of the surface area obtained by other researchers were of 13.2 (26), 1.2–5.2 (27), and 36.7–126 $m^2 \cdot g^{-1}$ (28).

Considerations on the Removal by Adsorption

The adsorption tests have been carried out in order to evaluate the equilibrium constants of adsorption. The influence of contact time on dye removal by $MgAl_2O_4$ is presented in Fig. 5. It can be seen that the material is efficient at absorbing dye, and the process gradually attains equilibrium. The time profile of dye removal is a single, smooth and continuous curve leading saturation, suggesting also the possible monolayer coverage of dye on the particle surface. Figure 5 shows also that the contact time required in attaining equilibrium is about 60 min for all the initial concentrations of the dye.

Several models of adsorption kinetics based on diffusional mass transport have been reported in the literature (29–31). Adsorption kinetic data were treated in this work using the film and pore diffusion model. In the heterogeneous adsorption sequence, mass transfer of dye molecules first takes place from the bulk fluid to the external surface of the spherical particles. The dye molecules then diffuse from the external surface into

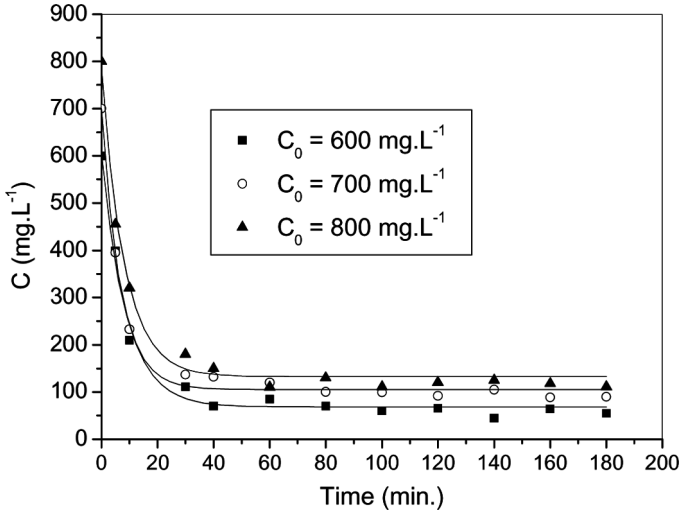

Figure 5. Kinetics adsorption of Direct Black 38 on $MgAl_2O_4$ with different initial dye concentrations ($MgAl_2O_4 = 1\,g \cdot L^{-1}$; pH = 2.5; T = 25°C).

and through the pores with the particle, within the adsorption taking place only on the solid surface of the pores.

The mass balance in the adsorbent spherical particle is given by Equation (1).

$$\varepsilon_p \cdot \frac{\partial C_i}{\partial t} = D_{ef} \cdot \left(\frac{\partial^2 C_i}{\partial r^2} + \frac{2}{r} \frac{\partial C_i}{\partial r} \right) - \frac{\partial q_i}{\partial t} \tag{1}$$

The initial and boundary conditions are given by Equations (2–4).

$$t = 0 \quad C_i = 0 \tag{2}$$

$$r = 0 \qquad \frac{\partial C_i}{\partial r} = 0 \tag{3}$$

$$r = R \quad \frac{dC_i}{dr} = \frac{K_f}{D_{ef}} \cdot (C_i - C_B) \tag{4}$$

Since the equilibrium isotherm can be described according to the Langmuir model:

$$\frac{\partial q_i}{\partial t} = \frac{q_m \cdot K_d}{(K_d - C_i)^2} \cdot \frac{\partial C_i}{\partial t} \tag{5}$$

By combining Equations (1) and (5):

$$\frac{\partial C_i}{\partial t}\left(\varepsilon_{\mathrm{p}}+\frac{q_m\cdot K_{\mathrm{d}}}{(K_{\mathrm{d}}+C)^2}\right)=D_{\mathrm{ef}}\cdot\left(\frac{\partial^2 C_i}{\partial r^2}+\frac{2}{R}\cdot\frac{\partial C_i}{\partial r}\right) \tag{6}$$

The dimensionless parameter, Biot number (Bi), defines a relative ratio between the mass transfer in the film around the particle and the mass transfer inside the particle (Equation (7)).

$$\mathrm{Bi}=\frac{K_{\mathrm{f}}.R}{D_{\mathrm{ef}}} \tag{7}$$

where R is the particle radius. When the Biot number is higher than 100, the major resistance to mass transfer is within the adsorbent particle rather than external to the particle.

The effective diffusivity in the pore diffusion model should be constant and equal to the pore diffusivity, which is also a function of molecular diffusivity, porosity and tortuosity, defined in Equation (8) (32). The effective diffusivity accounts for the fact that the diffusion paths are tortuous, the pores are of varying cross-sectional areas, and not all to the area normal to the direction of the flux is available (i.e., void) for the molecules to diffuse (32).

$$D_{\mathrm{ef}}=\frac{D_{\mathrm{M}}\cdot\varepsilon_{\mathrm{p}}}{\tau} \tag{8}$$

The tortuosity (τ) is defined as the relationship between the actual distance a molecule travels between two points inside the pores and the shortest distance between those two points (33). Porosity (ε_{p}) of the adsorbent $MgAl_2O_4$ was determined as 0.7 and the tortuosity is assumed to be equal to 1 (34). The molecular diffusivity (D_{M}) of the direct dye was estimated using the Wilke-Chang expression (Equation (9)), and it is shown in Table 1.

$$D_{\mathrm{M}}=\frac{\left(7.4\cdot 10^{-8}\right)(\phi\cdot M)^{0.5}T}{\mu\cdot V_m^{0.6}} \tag{9}$$

The film diffusion coefficient (K_{f}) was evaluated according to Equation 10 ($K_{\mathrm{f}}=1.4\times 10^{-2}\,\mathrm{cm}\cdot\mathrm{s}^{-1}$).

$$V\left[\frac{dC}{dt}\right]_{t=0}=-K_{\mathrm{f}}\cdot a\cdot(C-C_s)_{t=0} \tag{10}$$

Table 1. Predicted results for the adsorption of direct dye onto $MgAl_2O_4$ using theoretical film and pore diffusion model

C_0 ($mg \cdot L^{-1}$)	D_{ef} ($cm^2 \cdot s^{-1}$)
600	1.15×10^{-7}
700	1.08×10^{-7}
800	1.22×10^{-7}
–	3.1×10^{-7}[a]

[a]Calculated according to Equation (8).
D_{ef} effective diffusion coefficient.
C_0 initial dye concentration.

Figure 5 shows the decay curves of the sorption of dye with different initial dye concentrations. The curves are generated by solving Equations (1–6), and the D_{ef} values for each initial dye concentration are given in Table 1. Figure 5 shows an excellent agreement between the predicted and the experimental data, and the adjusted D_{ef} values are similar to that evaluated by Equation (9), and independent on the initial dye concentration (Table 1).

The Biot number is high (>100) and indicates that the film around the particle has negligible resistance to mass transfer of dye to the particle surface (35).

Figure 6 shows the adsorption isotherm that expresses the adsorbed amounts as a function of equilibrium concentration for Direct Black 38 in solution. Using the Giles classification (36), the isotherm obtained in

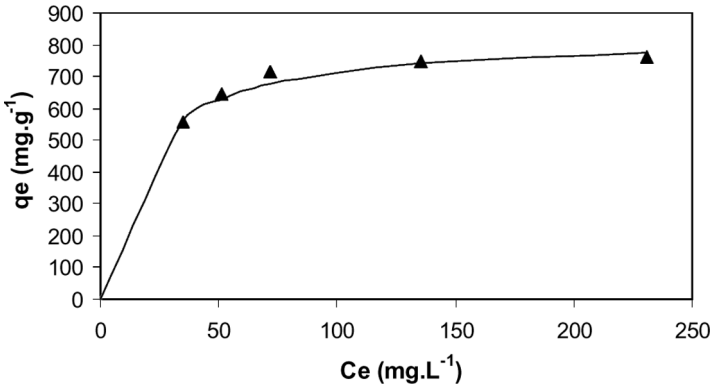

Figure 6. Direct Black 38 adsorption isotherm on $MgAl_2O_4$. (pH = 2.5; T = 25°C). Circle data points correspond to the experimental data and the line is the fitting to the Langmuir model.

the present work is the Langmuir type (L) with an initial concavity to the concentrations axis. The L-shape isotherm mean that there is no strong competition between the solvent and the dye to occupy the $MgAl_2O_4$ surface sites.

The data obtained from the adsorption experiments were fitted to the Langmuir model: (Eq. (10)) (37):

$$q_e = \frac{q_m b C_e}{1 + b C_e} \tag{10}$$

were C_e is the concentration of the dye in solution at equilibrium ($mg \cdot L^{-1}$), q_e is the amount of dye adsorbed per unit weight of the solid at equilibrium ($mg \cdot g^{-1}$), b is the Langmuir adsorption constant ($L \cdot mg^{-1}$), and q_m is the amount of dye adsorbed corresponding to monolayer coverage ($mg \cdot g^{-1}$).

The liner plot of $1/q_e$ *versus* $1/C_e$ (Fig. 7) show that adsorption follows Langmuir isotherm model. The fitting of experimental data to the Langmuir model resulted in maximum adsorption capacity (q_m) of $833\,mg \cdot g^{-1}$ and $b = 0.0597\,L \cdot mg^{-1}$. In a previous work, Moreira et al. (23) found a value of $q_m = 154\,mg \cdot g^{-1}$ for the adsorption of dye Direct Black 38 on commercially available Degussa TiO_2-P25 titanium dioxide, under the same experimental conditions employed in this work. The high value of q_m indicates that the $MgAl_2O_4$ spinel has an excellent ability to the removal of dyes in aqueous solution, which may be attributed to great specific surface area ($206.5\,m^2 \cdot g^{-1}$). The lager surface area benefits the

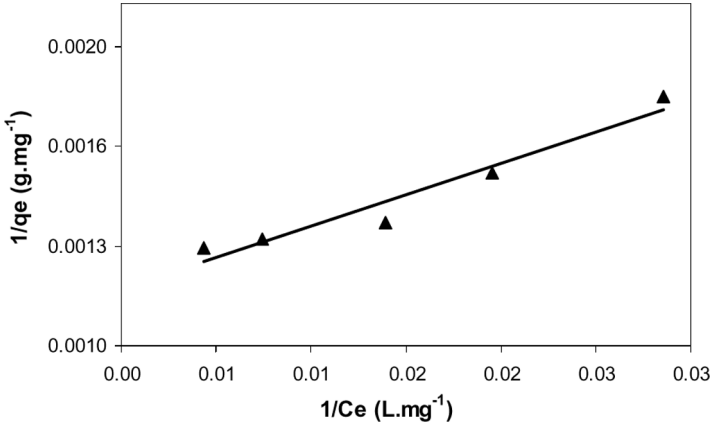

Figure 7. Langmuir model.

contact between dyes and solids surface and can absorb larger numbers of dye molecules.

CONCLUSIONS

The $MgAl_2O_4$ spinel was prepared successfully by low temperature process. The synthesized material presents a pure phase and the mean size of nanocrystal is of nanometric scale, and has high surface area. The adsorption kinetics was elucidated using the film and pore diffusion model, and the results showed that the diffusion of the dye in the film around the particle was faster than the internal diffusion. The adsorption isotherm was described according to the Langmuir model, and the monolayer coverage capacity was 833 mg of dye per gram of Zn_2SnO_4. The result indicate that $MgAl_2O_4$ could be employed for the dyes removal in aqueous solutions.

ACKNOWLEDGMENTS

The authors are grateful to the Brazilian research funding, CNPq, for the financial support.

NOMENCLATURE

q_m	maximum amount of dye adsorbed in the solid phase
b	Langmuir equilibrium constant
q_e	concentration of dye in the solid phase at equilibrium
C_B	concentration of dye in the aqueous phase at time t
C_e	concentration of dye in the aqueous phase at equilibrium
C_i	concentration of dye in the aqueous phase inside the particle
C_s	concentration of dye at surface ot the solid
D_{ef}	effective diffusion coefficient
D_M	molecular diffusivity
K_f	mass transfer coefficient in the hydrodynamic film around the particle
M	molecular weight
R	particle radius
r	radial position in relation to the center of the particle
t	time
T	temperature
V_m	molar volume

μ viscosivity
τ tortuosity
ϕ constant ($H_2O = 2.27$)
ε_p particle porosity
Bi Biot number
a relation between a sphere surface area and its volume

REFERENCES

1. Reife, A.; Fremann, H.S. (1996) *Environmental Chemistry of Dyes and Pigments*, 1st Ed., John Wiley Inc..
2. Papic, S.; Koprivanac, N.; Bozic, A.L. (2000) Removal of reactive dyes from wastewater using Fe(III) coagulant. *J. Soc. Dyers Color.*, *116* (11): 352.
3. Zhang, M.; An, T.; Hu, X.; Wang, C.; Sheng, G.; Fu, J. (2004) Preparation and photocatalytic properties of a nanometer ZnO–SnO2 coupled oxide, *Appl. Catal. A: Gen.*, *260* (2): 215.
4. Karadag, D.; Tok, S.; Akgul, E.; Ulucan, K.; Evden, H.; Kaya, M. (2006) Combining adsorption and coagulation for the treatment of azo and anthraquinone dyes from aqueous solution. *Ind. Eng. Chem. Res.*, *45* (11): 3969.
5. Mohorcic, M.; Teodorovic, S.; Golob, V. (2006) Fungal and enzymatic decolourisation of artificial textile dye baths. *Chemosph.*, *63* (10): 1709.
6. Bielska, M.; Prochaska, K. (2007) Dyes separation by means of cross-flow ultrafiltration of micellar solutions. *Dyes and Pigments*, *74* (2): 410.
7. Tan, I.A.W.; Ahmad, A.L.; Hameed, B.H. (2008) Adsorption of basic dye on high-surface-area activated carbon prepared from coconut husk: Equilibrium, kinetic and thermodynamic studies. *J. Hazard. Mater.*, *154* (1–3): 337.
8. Tamai H.; Yoshida, T.; Sasaki, M.; Yasuda, H. (1999) Dye adsorption on mesoporous activated carbon fiber obtained from pitch containing yttrium complex. *Carbon*, *37* (6): 983.
9. Miyamoto, N.; Kawai, R.; Kuroda, K.; Ogawa, M. (2000) Adsorption and aggregation of a cationic cyanine dye on layered clay minerals. *Appl. Clay Sci.*, *16* (3–4): 161.
10. Meshko, V.; Markovska, L.; Mincheva, M.; Rodrigues, A.E. (2001) Adsorption of basic dyes on granular acivated carbon and natural zeolite. *Water research*, *35* (14): 3357.
11. Wong, Y.C.; Szeto, Y.S.; Cheung, W.H.; McKay, G. (2003) Equilibrium Studies for acid dye adsorption onto chitosan. *Langmuir*, *19* (19): 7888.
12. Abdullah, A.G.L.; Salleh, M.A.M.; Mazlina, M.K.S.; Noor, M.J.M.; Osman, M.R.; Wagiran, R.; Sobri, S. (2005) Azo dye removal by adsorption using waste biomass: Sugarcane bagasse. Internat. *J. Eng. Techn.*, *2* (1): 8.
13. Chandrasekhar, S.; Pramada, P.N. (2006) Rice husk ash as an adsorbent for methylene blue: Effect of ashing temperature. *Adsorption*, *12* (1): 27.
14. Karadag, D.; Akgul, E.; Tok, S.; Erturk, F.; Kaya, M.; Turan, M. (2007) Basic and reactive dye removal using natural and modified zeolites. *Chem. Eng. Data*, *52* (6): 2436.

15. Saito, F.; Kim, W. (1999) Effect of grinding on synthesis of $MgAl_2O_4$ spinel from a powder mixture of $Mg(OH)_2$ and $Al(OH)_3$. *Powder Technol.*, *113* (1–2): 109.
16. Dung, T.W.; Ping, L.R.; Azad, A.M. (2001) Magnesium aluminate ($MgAl_2O_4$) spinel produced via self-heat-sustained (SHS) technique. *Mater. Res. Bull.*, *36* (7–8): 1417.
17. Aglietti, E.F.; Mazzoni, A.D.; Sainz, M.A.; Caballero, A. (2002) Formation and sintering of spinel ($MgAl_2O_4$) in reducing atmospheres. *Mater. Chem. Phys.*, *78* (1): 30.
18. Bakkar, W.; Lindsay, J.G. (1967) Reactive magnesia spinel, preparation and properties, Am. *Ceram. Soc. Bull.*, *46* (11): 1094.
19. Huang, H.; Kong, L.B.; Ma, J. (2002) $MgAl_2O_4$ spinel phase derived from oxide mixture activated by a high-energy ball milling process, *Materials Letters*, *56* (3): 238.
20. Bratton, R.J. (1969) Co-precipitates yielding $MgAl_2O_4$ spinel powders. *Am. Ceram. Soc. Bull.*, *48* (12): 759.
21. Shiono, T.; Shiono, K.; Miyamoto, K.; Pezzotti, G. Synthesis and characterization of $MgAl_2O_4$ spinel powder from a heterogeneous alkoxide solution containing fine MgO powder, *J. Am. Ceram. Soc.*, *83* (1): 235.
22. Walker, D.; Walker Jr., E.H.; Owens, J.W.; Etienne, M. (2002) The novel low temperature synthesis of nanocrystalline $MgAl_2O_4$ spinel using gel precursors. *Mater. Letters*, *37* (6): 1041.
23. Moreira, R.F.P.M.; Sauer, T.P.; Casaril, L.; Humeres, E. (2005) Mass transfer and photocatalytic of leather dye using TiO_2/UV. *J. Appl. Eletroch.*, *35*: 821.
24. Adak, A.K.; Saha, S.K.; Pramanik, P. (1997) Synthesis and characterization of $MgAl_2O_4$ spinel by PVA evaporation technique. *J. Mater. Sci. Letters*, *16* (3): 234.
25. Guo, J.; Lou, H.; Zhao, H.; Wang, X.; Zheng, X. (2004) Novel synthesis of high surface area $MgAl_2O_4$ spinel as catalyst support. *Mater. Letters*, *58* (12–13): 1920.
26. Tripathi, S.; Mukherjee, B.; Das, S.; Haldar, M.K.; Das, S.K.; Ghosh, A. (2003) Synthesis and densification of magnesium aluminate spinel: Effect of MgO reactivity. *Ceram. Internat.*, *29* (8): 915.
27. Thanabodeekija, N.; Sathupunya, M.; Jamieson, A.M.; Wongkasemjit, S. (2003) Correlation of sol–gel processing parameters with microstructure and properties of a ceramic product. *Mater. Characteriz.*, *50* (4–5): 325.
28. Ganesh, I.; Johnson, R.; Rao, G.V.N.; Mahajan, Y.R.; Madavendra, S.S.; Reddy, B.M. (2005) Microwave-assisted combustion synthesis of nanocrystalline $MgAl_2O_4$ spinel powder. *Ceram. Internat.*, *31* (1): 67.
29. Spahn, H.; Schlunder, U. (1975) The scale-up of activated carbon columns for water purification based on results from batch test I. Theoretical and experimental determination of adsorption rates of single organic solutes in batch tests. *Chem. Eng. Sci.*, *30*: 529.
30. Neretnieks, I. (1974) Adsorption of components having a saturation. Isotherm. *Chem. Ing. Technol.*, *46*: 781.

31. Chen, B.; Hui, C.W.; McKay, G. (2000) Pore-surface diffusion modeling for dyes from effluents on pith. *Langmuir*, *17*: 740.
32. Choy, K.K.H.; Porter, J.F.; McKay, G. (2004) Film-pore diffusion models – analytical and numerical solutions. *Chem. Eng. Sci.*, *59*: 501.
33. Levenspiel, O. (1962) *Chemical Reaction Engineering*, Wiley, New York.
34. Gaffney, A.M. (June 11, 2002) Catalytic partial oxidation process and promoted nickel based catalysts supported on magnesium oxide U.S. Patent 6,402,989.
35. Ko, D.C.K.; Porter, J.F.; McKay, G. (2001) Film-pore diffusion model for the fixed-bed sorption of copper and cadmium ions onto bone char, *Water Res.*, *35* (16): 3876.
36. Giles, C.H.; D́Silva, A.P.; Easton, I.A. (1974) A general treatment and classification of the solute adsorption isotherm. II. Experimental interpretation. *J. Colloid Interface Sci.*, *47*: 766.
37. Langmuir, I. (1918) The adsorption of gases on plane surfaces of glass, mica and platinum. *J. Am. Chem. Soc.*, *40*: 1361.